

ANNEALING EFFECTS ON UNDOPED AND Co DOPED ZnO PELLETS SYNTHESIZED BY DC THERMAL PLASMA METHOD

Dr. M. Nirmala* & Dr. A. Anukaliani**

- * Assistant Professor, Department of Physics, Sri GVG Visalakshi College for Women, S.V Mills Post, Udumalpet, Tamilnadu
- ** Associate Professor, PG and Research Department of Physics, Kongunadu Arts and Science College, Coimbatore, Tamilnadu

Cite This Article: Dr. M. Nirmala & Dr. A. Anukaliani, "Annealing Effects On Undoped and Co Doped ZnO Pellets Synthesized By DC Thermal Plasma Method", International Journal of Advanced Trends in Engineering and Technology, Page Number 101-110, Volume 2, Issue 1, 2017.

Abstract:

Nano-sized ZnO and Co doped ZnO was synthesized through the DC thermal plasma method. The synthesized nanoparticles are characterized for their phase and morphology by X-ray diffraction (XRD), scanning electron microscopy (SEM) and transmission electron microscopy (TEM). The XRD studies show the formation of hexagonal phase pure ZnO with c-axis preferred orientation. The doping of Co ions in ZnO was confirmed by observation of absorption band edges at in the UV-vis spectra of the samples. The pellets from this powder have been calcined at temperatures 450°C, 550°C and 650°C for one hour. Keithley source unit was used to study the DC characteristics of the ZnO pellets in the range from room temperature to 100°C with a step of 25°C. From Arrhenius plot, it is found that the activation energy for electrical transport is maximum (1eV) when calcinations are performed at the temperature 650°C. The present work is of particular significance for the preparation of undoped and Co doped nanoparticles for studies of their electrical and optical properties with respect to their wide range of potential applications.

Key Words: Zinc Oxide, Nano-Size, Electrical Properties, Cobalt & Doping

1. Introduction:

Zinc oxide (ZnO) is a wide-band gap semiconductor that is desirable for many applications, such as piezoelectric transducers, varistors, gas sensors and transparent conducting thin films [1-3]. By reducing the size of ZnO crystals to nanoscale dimensions or controlling the morphology of ZnO crystals to tetra pod-shaped nanowhiskers [4], nanowires and nanorods [5] researches can tailor the properties via quantum confinement and surface effect. To date various techniques have been used to synthesize ZnO nanoparticles including chemical or physical methods [6]. The former are thermal hydrolysis technique [7], hydrothermal processing [8], and sol—gel method [9-11]. The latter are spray pyrolysis [12], vapor condensation method [13] and thermo chemical decomposition of metal organic precursors [14]. Nevertheless, the main problems of most methods have been the poor throughput efficiency and the difficulty in size control.

In this paper, we report a rapid fabrication technique of undoped and Co doped ZnO nanopowders by dc thermal plasma synthesis with a high production rate. By changing gas combination and the gas flow rate, different morphology and varied growth rate of the ZnO nanopowders can be achieved. The interest in doping ZnO is to explore the possibility of tailoring its electrical, magnetic and optical properties [15-19]. In this study, characterization of pure and Co ZnO and activation energy of electron transport of the samples produced at different annealing temperatures has been evaluated.

2. Experiment:

In the present study, a novel dc plasma reactor operated at 7kW and atmospheric pressure was used to synthesize pure and Co doped ZnO nanoparticles. Commercial zinc powder with an average particle size of 10 µm and containing impurities of Cr Fe and Pb less than 50 ppm were used as the raw material. The Zn powders were fed into plasma flame through air and subsequently underwent vaporization, oxidation and quench processes. Dop- ing cobalt into ZnO nanoparticles was achieved by introducing cobalt metal powder into the plasma-forming. The prepared powder was collected from the Hood and chamber part. A flow rate of the plasma was in the range of 15 l/min, an oxidation reaction took place in the flame of the plasma.

The phase identity and crystallite size of the ZnO nanoparticles were determined using an X-ray diffractometer (XRD, Philip PW1700) operated at 40 keV and 40mA with CuK_{α} radiation. A scanning electron microscope (SEM) and transmission electron microscope (TEM, Jeol 2010) were used for morphological observations of the pure and Co doped ZnO nanoparticles. The chemical composition of the nanoparticles was analyzed by energy dispersive x-ray (EDAX) analysis. The optical properties of the samples were investigated by measuring the UV-Vis absorbance spectra at room temperature.

Keithley 236 Source Measure Unit attached with an indigenously designed and fabricated four probe sample holder was used to study the DC characteristics of the ZnO nanoparticles in the range RT to 100° C with a step of 10° C. The samples were used in the form of circular pellets of diameter 0.8 cm and 0.4 cm thickness.

3. Results and Discussion:

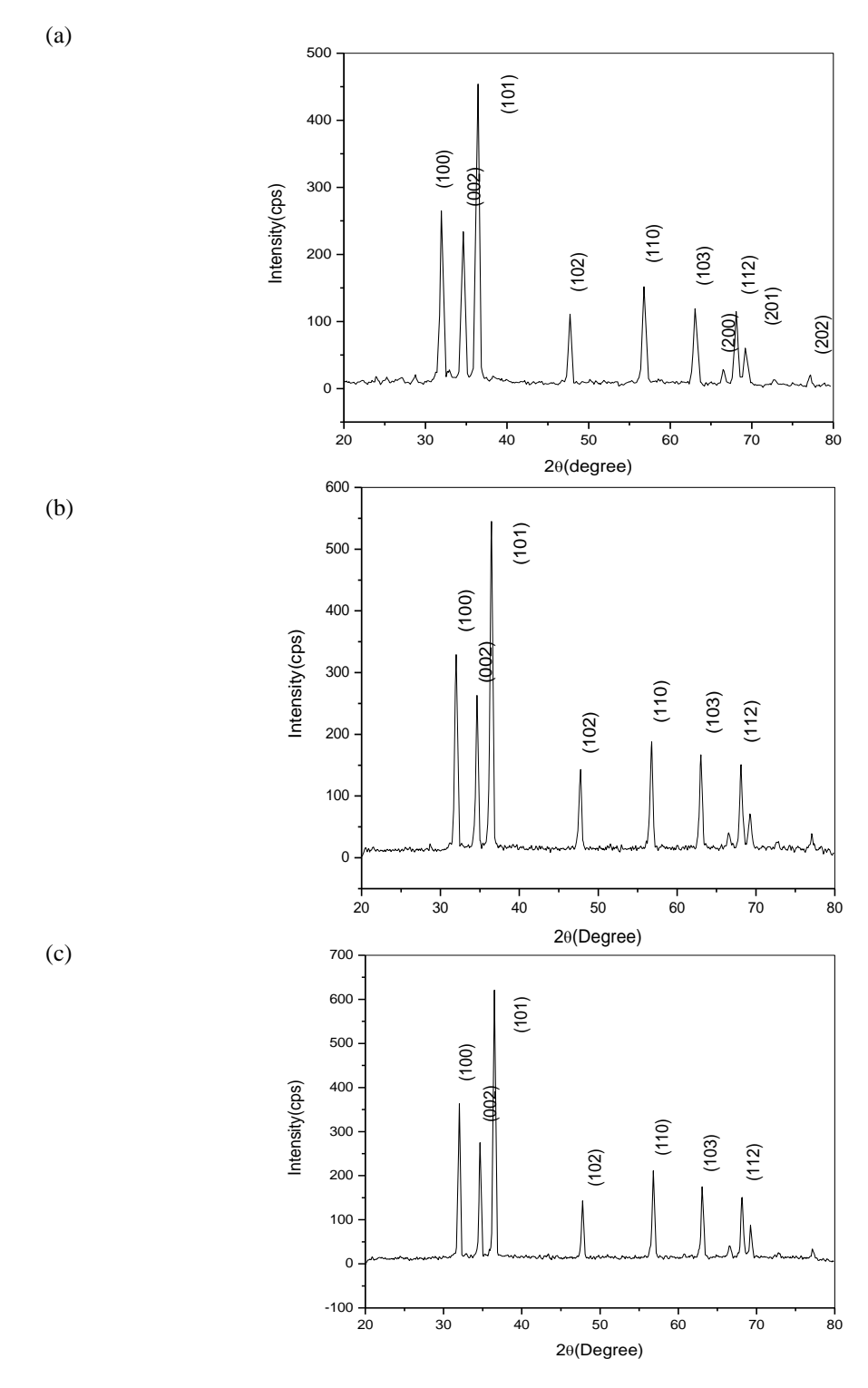


Figure 1

Figure 1a, 1b and 1c shows the XRD patterns of undoped and 5, 10 at% Co doped ZnO nanoparticles where all samples show similar diffraction peak positions. No peaks were observed as phases of Co clusters and impurities, indicating high purity of the ZnO nanopowders obtained by dc thermal plasma synthesis. The strong intensities relative to the background signal also indicated high crystallization quality of the ZnO nanopowders. It can be see that all peaks in undoped and Co doped ZnO samples could be fitted with wurtzite structure (space group $P6_3mc$ (No.186) (JCPDS No. 36-1451)) [20]. After calculation from the XRD results, the average size of the undoped ZnO is found to be 26nm, and for 5 at% and 10 at% Co doped ZnO the average size is found to be

27 and 29nm respectively. It is seen that, compared with undoped ZnO, Cobalt doping in ZnO samples resulted in an increase of crystalline size. The same results were also reported by Huaming Yang and Sha Nie [21].

It is seen that as the doping concentration increases the values of lattice parameters 'a' and 'c' decreases compared to undoped ZnO. The difference in radii between divalent, high-spin Co in tetrahedral coordination (0.58\AA) and divalent Zn in tetrahedral coordination (0.60\AA) is very small [22]. As a consequence, changes in cell parameters and cell volume with cobalt substitution are also small. Interestingly, the substitution results in a decrease in a and c parameter in keeping with the smaller radius of Co^{2+} . If the Co^{2+} ions were in an octahedral environment in the wurtzite structure, it would have shown a significant increase in the cell parameters since octahedral Co^{2+} has a radius between $0.65\text{\AA}(\text{low spin})$ and $0.745\text{\AA}(\text{high spin})[23]$.

Fig 2a, 2b&2c and 3a, 3b& 3cshows the XRD patterns of 5,10 at % Co doped ZnO pellets annealed at 450° C, 550° C and 650° C respectively. The calculated

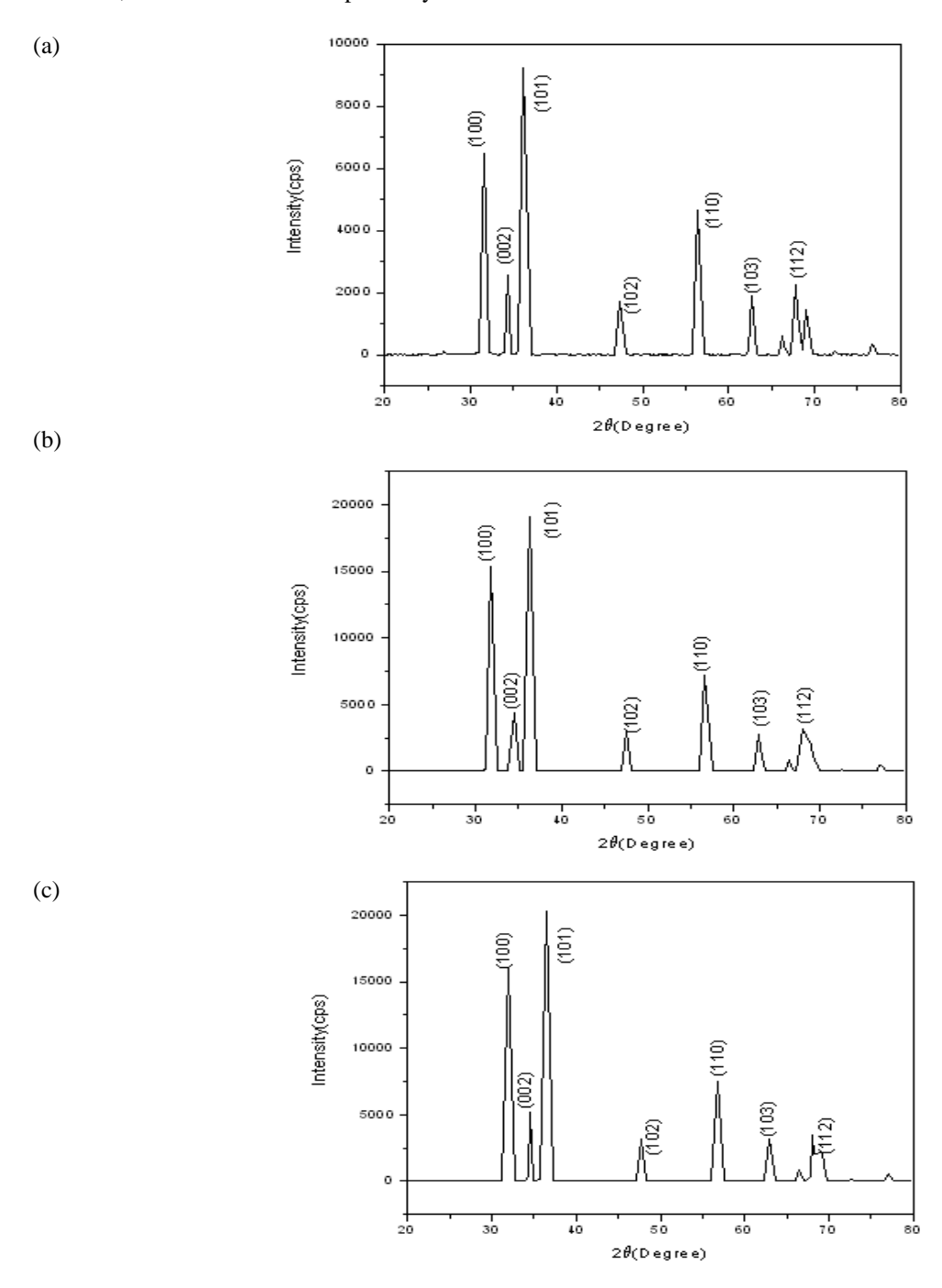
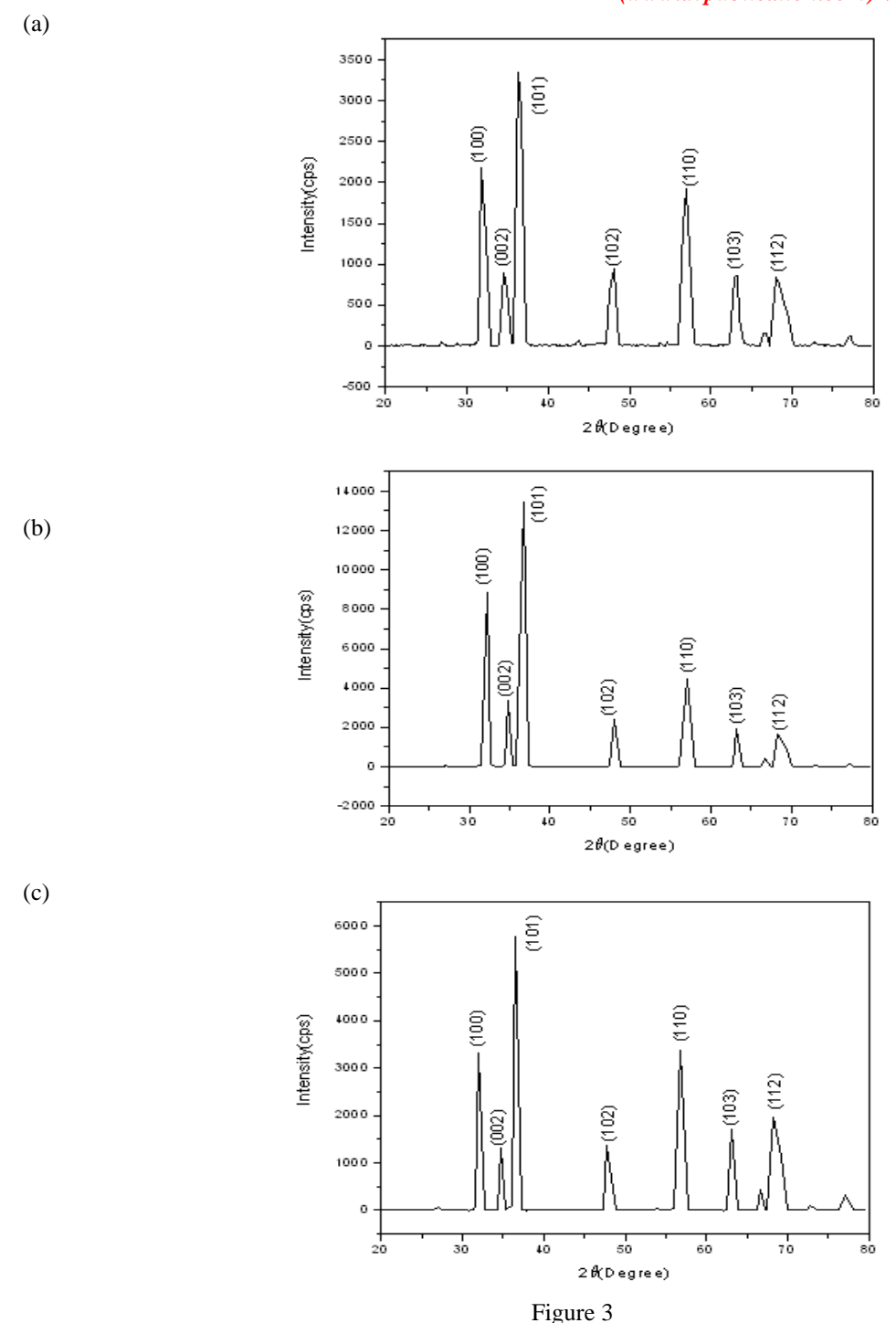
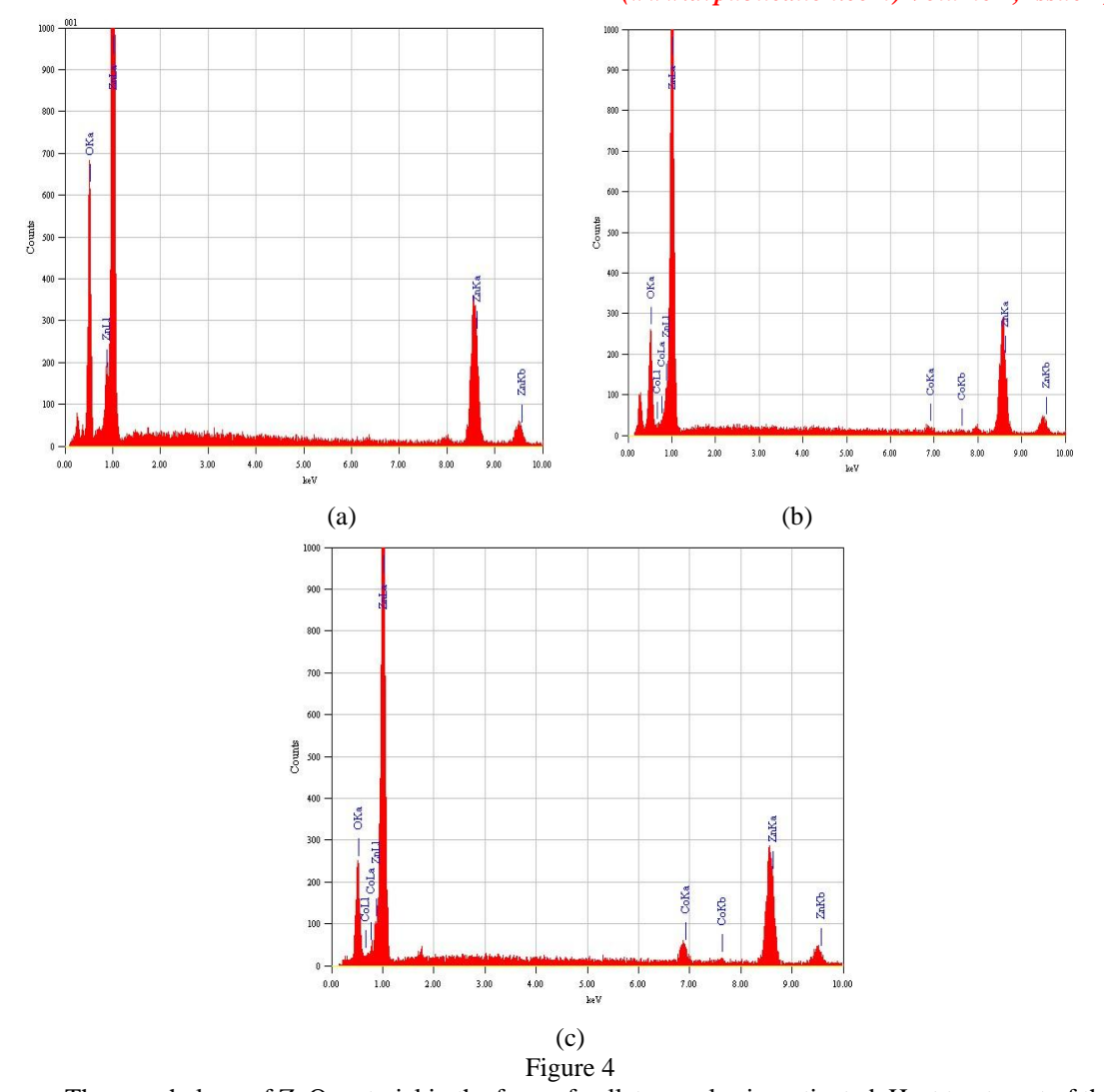


Figure 2

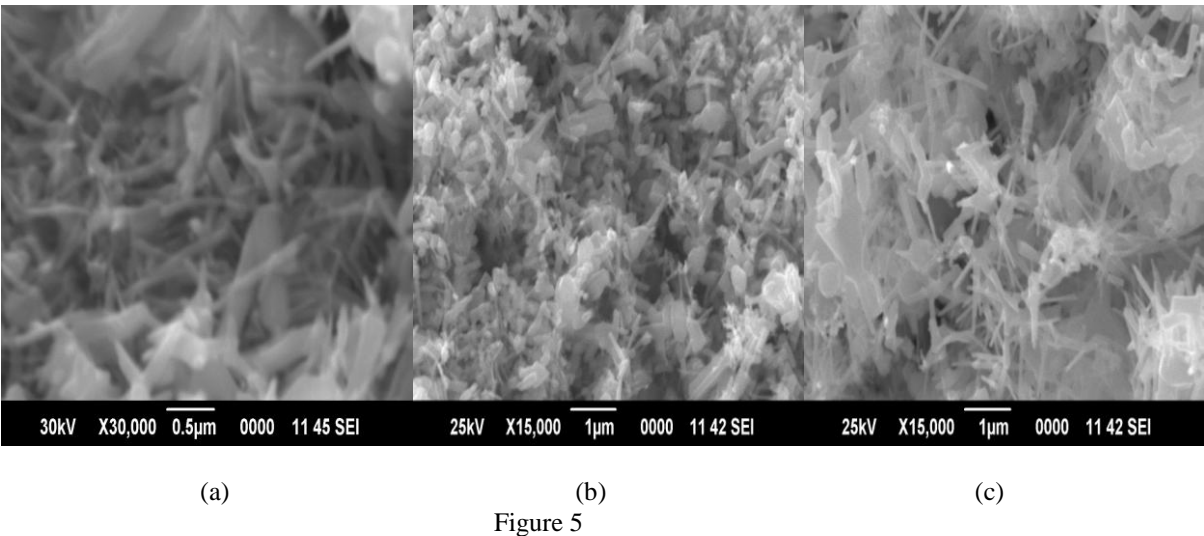


Crystallite sizes are 24, 26 and 29nm annealed at 450°C, 550°C and 650°C respectively in the case of undoped ZnO and for 5,10 at % Co doped ZnO was found to be 30,32,33 and 29,26,27nm respectively. It may be seen from the pattern [Fig 2&3] that as the annealing temperature increases the amount of impurities decreases and the material becomes purer and more crystalline.

In addition the composition analysis shows that the Co composition in ZnCoO sample is less compared with the nominal composition. So it is not easy for Co ions to enter the ZnO crystal structure, indicating that the ZnO growth process is in equilibrium state, to avoid inclusions of foreign phases [24]. Figure 4a, 4b and 4c shows the EDX spectrum of undoped and 5, 10 at% cobalt doped ZnO nanopowders respectively. Table 1 gives the ratio of Zn: Co: O elemental composition. The atomic percentages of the elements are obtained from the spectra and the doping of cobalt is confirmed. Formations of a dominant nano needle like crystal population have been observed from the SEM analysis of undoped and Co doped ZnO nanopowders which are shown in figure 5a, 5b & 5c.



The morphology of ZnO material in the form of pellet was also investigated. Heat treatment of the ZnO element at different temperatures gave different morphology of material. Fig.6a-6c shows the morphology of 5 at % Co doped ZnO in the form of pellet annealed at 450C, 550C and 650C respectively. It is found that with increase in temperature, material has become more porous. SEM studies show that the material has networks of nanosheet [25].



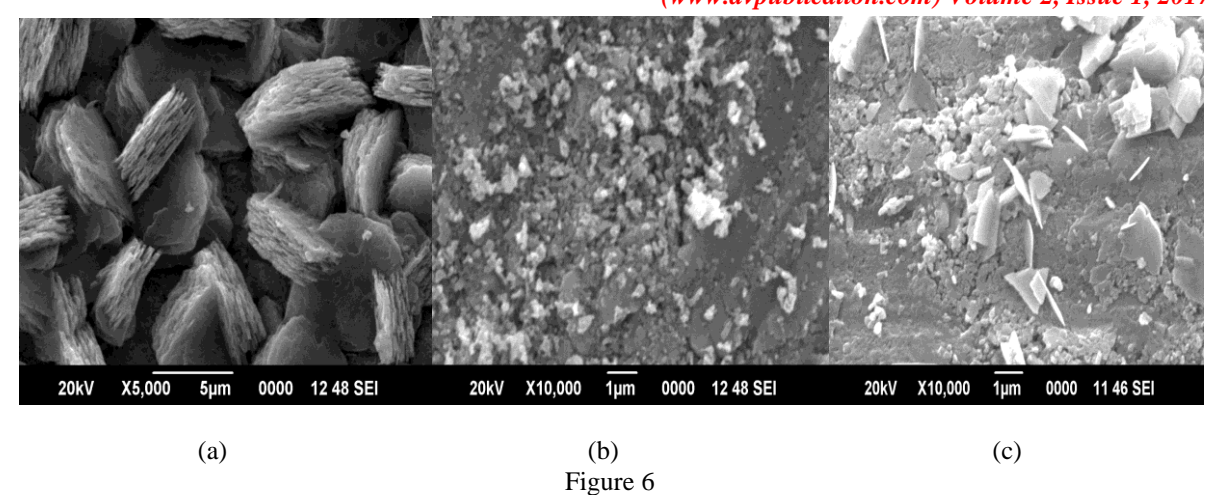


Figure 7 shows the UV-Vis absorption spectra of ZnO with different Co concentration. The absorption edge takes the value at 284 nm from the absorption curve. This indicates a blue shift in the spectrum. Kumbhakar *et al.*, has reported that the excitonic absorption peak observed at 262 nm due to ZnO nanoparticles lies much below the band gap wave length of bulk ZnO (388 nm), and the sharpness of the peak indicates monodispersed nature of nanoparticles distribution. In the spectrum, the absorption peak of ZnO at 284 nm may be due to the monodispersion of nanoparticles [26].

The absorption edge of 5at% and 10at% Co doped ZnO are 361, 351nm respectively. The position of the absorption spectra is observed to shift towards the lower wavelength side with increasing Co doped concentration in ZnO. This indicates that the band gap of ZnO material increases with the doping concentration of Co²⁺ ion. The increase in the band gap or blue shift can be explained by the Burstein – Moss effect [27]. This is the phenomenon that the Fermi level merges into the conduction band with increase of the carrier concentration. Thus the low energy transitions are blocked. The results are in good agreement with the results reported by K. Sakai *et al.* [28].

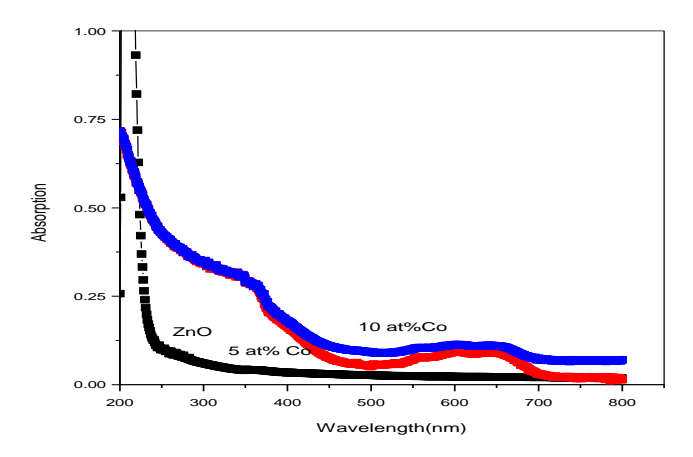


Figure 7

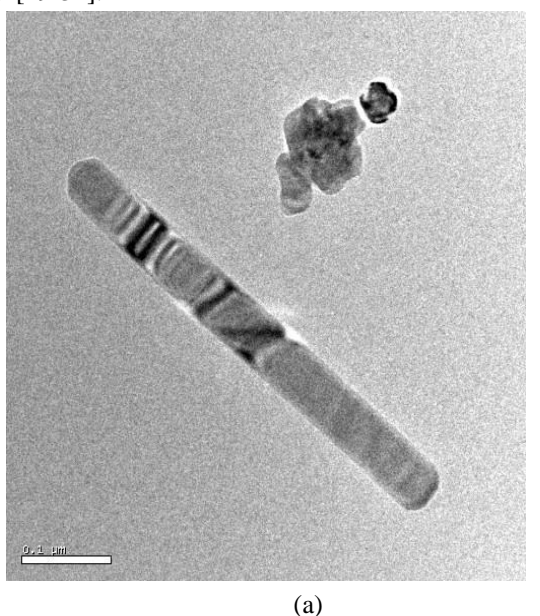
Figure 8 shows the transmission electron microscopy (TEM) images of Co doped ZnO nanorods. It can be observed from the images that the Co doped ZnO nanorods have smooth sidewalls and uniform diameters. The average diameter and length of pure and Co doped ZnO nanorods are about 3nm and 5nm respectively. The HRTEM investigates that the interspacing between crystal planes for both samples is 0.52nm and growth direction is along [001], which provides explicit evidence that the synthesized samples grow along c-axis consistent with XRD results.

Temperature dependence of conductivity for n-type semiconductor material can be expressed as,
$$\sigma \!\! = \sigma_0 e^{\text{-}Ea/KT}$$

Where $\sigma_0=2$ $e\mu_e(2\Pi m_e^*(KT/h^2))^{3/2}$ and $E_a=E_c-E_i$. Here m_e^* is the effective mass and μ_e is the mobility of electron. E_a , E_c and E_i are the energy value corresponding to activation of electronic transport, bottom edge of the conduction band and level of the donor state. T is the absolute temperature of material, e is the electronic charge, h is Planck's constant and k is the Boltzmann constant.

In terms of resistance Eq. (1) is given by
$$R = R_0 e^{Ea/KT} \eqno(2)$$

From the resistance temperature plot (fig 9a, 9b& 9c) in the form of ln(R) versus 1/T the slope gives the value of (E_a/k) of Eq. (2) and evaluates the activation energy of electronic transport for semi conducting material [29-31].



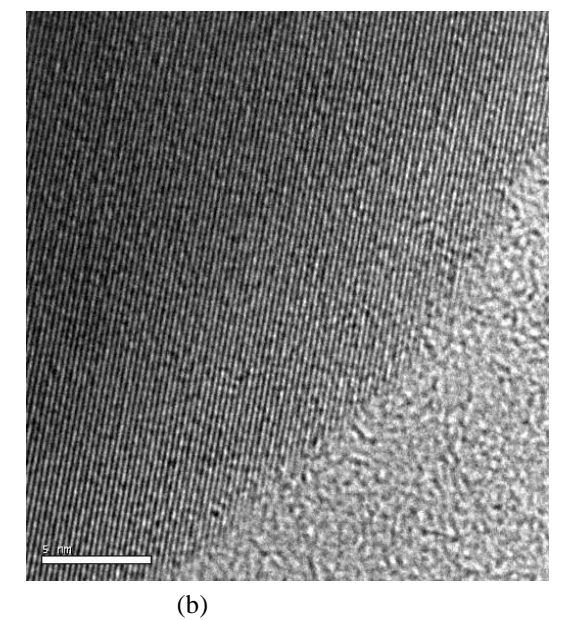
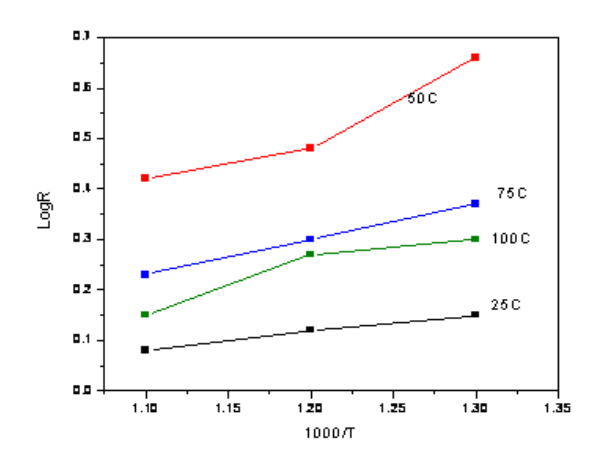
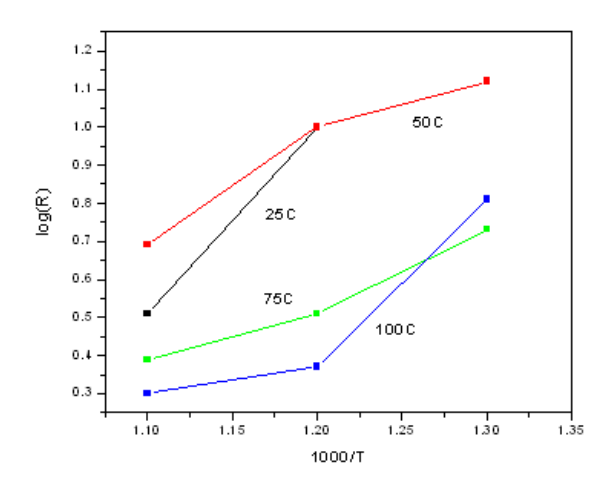


Figure 8

One of the important variables resulting from the electric properties of semiconductors is the activation energy. This is the initial energy that the electric charges need to move inside the material. Activation energy increases with temperature in insulators and semiconductors and decreases in metals. It is well known that electrical conduction can take place by means of two parallel processes namely band conduction and hoping conduction. The band conduction occurs when the carriers are excited beyond the mobility edges into non-localized states at high temperatures. The excitations of carriers into localized states at band edges cause the hoping conduction [32].

The resistance-temperature characteristics of undoped and 5, 10 at % Co doped ZnO nanomaterial synthesized by dc thermal plasma method is shown in figures 9a, 9b and 9c. The activation energy values calculated from the plot and their corresponding temperature range are tabulated in Table 2. Table 2 shows that, the activation energy for electronic conduction of the ZnO nano-material increases with an increase in temperatures given to the sample. This is possible due to change in surface chemical structure of oxide. The removal of defects in crystallites correspondently with an increase in activation energy with the rise in annealing temperatures. It is also observed that as the annealing temperature increases the resistance of the material decreases. This is probably due to growth crystallites. At any temperature the Gibb's free energy of a crystal is minimum when a certain fraction of ions leaves the normal lattice. Yadav et al [25, 33] has reported that the sample annealed at higher temperature follow conduction of proton by hopping mechanism due to inadequate number of free hydroxyl groups on the surface having higher value of activation energy.





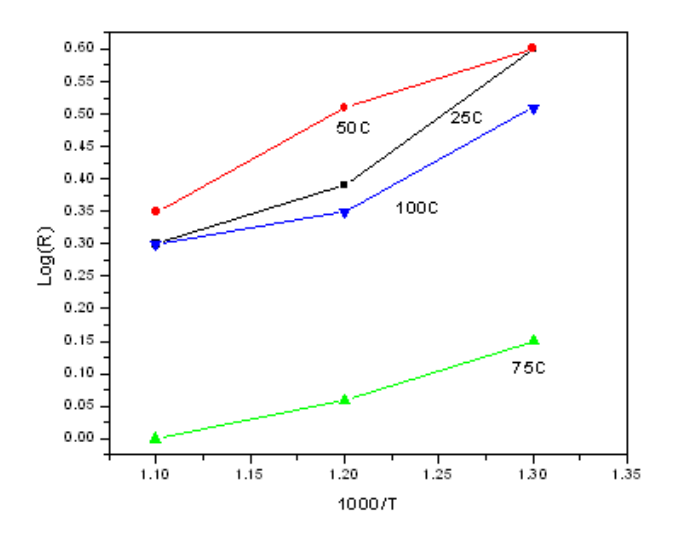


Figure 9

Computed values of activation energies from the plots ln R Vs 1000/T confirm higher values of activation energy in case of ZnO with Co doping. The increase in activation energy gives clue regarding the diffusion of impurities to the regular position or to the interstice [34]. The high value of the activation energy may be associated with ionization of deep donor or acceptor levels which become more important at higher temperature. With increasing temperature the concentration of conducting electrons increased and therefore the role of mutual interaction between electrons and donor or acceptor centers become more important [35].

Doping on semiconductor can modify resistance. The electrical conductivity increases with the increase in impurity concentration and temperature. The defect concentration will increase exponentially with temperature and consequently the electrical conduction also increases. The addition of impurity further increases the electrical conduction in the temperature region considered.

Table 1: Compositional analysis of ZnO and ZnCoO

Dopant Concentration	Experimental Results (Atomic %)			
	Zn	Co	0	
0 at %	23.14	-	76.86	
5 at %	27.13	0.93	71.93	
10 at %	28.50	2.84	68.66	

Table 2: Activation Energy (Electron Conduction)

Temperature/Sample	25	50	75	100
Un doped ZnO	0.4	0.5	0.6	1.0
5 at.wt % Co doped ZnO	0.2	0.4	0.8	1.7
10 at.wt % Co doped ZnO	0.9	0.9	1.0	1.6

4. Conclusion:

Co doped and undoped ZnO nanopowders were synthesized by dc thermal plasma method. The measurements of XRD, SEM with EDX analysis shows that as undoped ZnO samples were in a pure wurtzite structure and in the Co doped ZnO samples Co ions had substituted Zn sites. UV-Vis spectrum revealed that the position of the absorption spectra is observed to shift towards the lower wavelength side with increasing Co doped concentration in ZnO. The lattice fringe spacing in the HRTEM image is 5nm which corresponds to the hexagonal wurtzite structure of ZnO and indicates that the growth occurred along 001 direction. DC conductivity revealed that as the annealing temperature increases the resistance of the material decreases. This is probably due to the removal of defects in crystallites correspondently with an increase in activation energy with rise in annealing temperature. This property of synthesized ZnO pellets can be used for moisture sensing device applications.

5. Acknowledgements:

The authors are grateful to the Secretary, Director, Principal and Head of the Department of Physics, Sri G.V.G Visalakshi College for Women, Udumalpet for their excellent encouragement and support. The authors wish to thank Ion arc Tec Pvt Ltd, Coimbatore, India, for providing the hospitality and all the experimental facilities during the project work.

6. References:

1. Z. L. Wang, Zinc oxide nanostructures: growth, properties and applications, J. Phys. Condens. Matter. 16(2004)829-858.

- 2. D. C. Look, Recent advances in ZnO materials and devices, Mater. Sci. Eng. B. 80(2001), 383-387.
- 3. J. F. Wager, Transparent Electronics, Science. 300(2003)1245-1246.
- 4. R. Wu, C.S. Xie, H. Xia, J.H. Hu, A.H. Wang, The thermal physical formation of ZnO nanoparticles and their morphology, J. Cryst. Growth. 217 (2000) 274–280.
- 5. D. W. Zeng, C. S. Xie, B. L. Zhu, R. Jiang, X. Chen, W. L. Song, J. B. Wang J. Shi, Controlled Growth of ZnO Nanomaterials via Doping Sb, J. Crst. Growth. 266 (2004) 511-518.
- 6. K. J. Klabunde, Nanoscale Materials in Chemistry, John Wiley and Sons, New York, 2001, pp. 88.
- 7. H. K. Park, D.K. Kim, C.H. Kim, Effect of Solvent on Titania Particle Formation and Morphology in Thennal Hydrolysis of \$TiCL_4\$, J. Am. Ceram. Soc. 80 (1997) 743-749.
- 8. S. I. Hirano, Hydrothermal Processing of Ceramics, Ceram. Bull. 66 (1987) 1342-1344.
- 9. D. Vorkapic, T. Matsoukas, Effect of Temperature and Alcohols in the Preparation of Titania Nanoparticles from Alkoxides, J. Am. Ceram. Soc. 81 (1998) 2815-2820.
- 10. V. R. Palkar, Sol–gel derived nanostructured gamma-alumina porous spheres as an adsorbent in liquid chromatography, Nanostruct. Mater. 11 (1999) 369-374.
- 11. T.S. Ko, S. Yang, H.C. Hsu, C.P. Chua, H.F. Lin, S.C. Liao, T.C. Lu, H.C. Kuo, W.F. Hsieh, S.C. Wang, ZnO nanopowders fabricated by dc thermal plasma synthesis, Mater.Sci Eng B. 134 (2006) 54–58
- 12. T.T. Kodas, Generation of complex Metal Oxides by Aerosol Processes: Superconducting ceramic particles and films, Adv. Mater. 6 (1989) 180-192.
- 13. C.G. Granqvist, R.A. Burhman, Ultrafine metal particles, J. Appl. Phys. 47 (1976) 2200-2219.
- 14. G. Skanadan, Y.J. Chen, N. Glumac, B.H. Kear, Synthesis of Oxide Nanoparticles in Low Pressure Flames, Nanostruct. Mater. 11(1999) 149-153.
- 15. S. Major, A. Banerjee, K. L. Chopra, Highly transparent and conducting indium-doped zinc oxide films by spray pyrolysis, Thin Solid Films. 108(1983)333-340.
- 16. S. Major, A. Banerjee, K. L. Chopra, K.C.Nagpal, Thickness-dependent properties of indium-doped ZnO films, Thin Solid Films. 143(1986)19-30.
- 17. K. Hauffe, A. L. Vierk, Electrical conductivity of zinc oxide with foreign oxides, Phys Chem. 196 (1950)160-180.
- 18. C. Wagner, The mechanism of the decomposition of nitrous oxide on zinc oxide Catalyst, J Chem Phys. 18(1950)69-71.
- 19. A. F. Aktaruzzaman, G.L. Sharma, L.K.Malhotra, Electrical, optical and annealing characteristics of ZnO:Al films prepared by spray pyrolysis, Thin Solid Films. 198 (1991)67-74.
- O.D. Jayakumar, H.G. Salunke, R.M. Kadam, Manoj Mohapatra, G. Yaswant and S.K. Kulshreshtha, Magnetism in Mn-doped ZnO nanoparticles prepared by a co-precipitation method, Nanotechnology I.O.P. Publishing. 17 (2006) 1278-1285.
- 21. Huaming Yang, Sha Nie, Preparation and characterization of Co-doped ZnO Nanomaterials, Mater Chemi Phys. 114 (2009) 279-282.
- 22. R. D. Shannon, Acta Crystallogr. Sect. A: Cryst. Phys. Diffr. Theor. Gen. Crystallogr, A32 (1976)751.
- 23. O.D. Jayakumar , I.K. Gopalakrishnan , S.K. Kulshreshtha , The structural and magnetization studies of Co-doped ZnO co-doped with Cu : Synthesized by co-precipitation method, J. Matter. Chem.15 (2005) 3514-3518.
- 24. Xueyun Zhou, Shihui Ge, Dong Sheng Yao, Yalu Zuo, Yuhna Xiao, Preparation, magnetic and optical properties of ZnO and ZnO:Co rods prepared by wet chemical method, Journal of Alloys and Compounds. 463 (2008) L9-L11.
- 25. B.C.Yadav, Richa srivastava, C.D. Dwivedi, P.Pramanik, Synthesis of nano-sized ZnO using drop wise method and its performances as moisture sensor, Sensors and Actuators. A153 (2009)137-141.
- 26. P. Kumbhakar, D. singh, C. S. Tiwary, A. K. Mitra, Chemical synthesis and visible photoluminescence emission from monodispersed ZnO nanoparticles, Chalcogenide Letters. 5 (2008) 387-394.
- 27. Sumetha Suwanboon, Tunattha Ratana, Walailak Thanakorn Ratana, Effects of Al and Mn dopant on structural and optical properties of ZnO Thin film prepared by Sol-Gel route, J. Sci. and Tech., 4 (2007) 111-121.
- 28. K. Sakai, T. Kakeno, T. Ikari, S. Shirakata, T. Sakemi, K. Awai, T. Yamamoto, Defect centers and optical absorption edge of degenerated semiconductor ZnO thin films grown by a reactive plasma deposition by means of piezo electric photothermal spectroscopy, Journal of Applied Physics. 99 (2006) 043508-043514.
- 29. O.Lopatiuk, L. Chernyak, Lithium-related states as deep electron traps in ZnO Appl.Phys.Lett. 87(2005)2144110- 2144112.
- 30. Y. Ohbuchi, T. Kawahara, Y. Okamoto, J. Morimoto, Characterization of Interface States in Degraded ZnO Varistors, Jpn. J. Appl. Phys. 41(2002)190-196.

- S. Walbran, A. A. Kornyshev, Proton transport in polarizable water, J. Chem. Phy. 114 (2001)10039-10048
- 32. P. K. Jain, N. S. Saxeena, Temperature and composition dependence of electrical conductivity of Se90In10-xSbx (x=0, 2, 4, 6, 8, 10) chalcogenide glasses, Journal of Non Oxide and Photonic Glasses. 1(2009)43-52.
- 33. B. C. Yadav, Richa srivastava, C.D.Dwivedi, P.Pramanik, Moisture sensor based ZnO nanomaterial synthesized through oxalate route, Sensors and Actuators B. 131(2008) 216-222.
- 34. R. Ananda Kumari, R. Chandramani, Electrical conductivity and dielectric measurements in Au⁺ doped/undoped KDP crystals with KCl and NaCl as additives, Indian journal of pure and applied physics. 43(2005)123-128.
- 35. M. Serin, O. Cankurtaran, F. Yilmaz, Electrical conductivity measurements in the range of Temperature induced conformational transitions in undoped and doped glassy poly (phenyl sulfone), Journal of optoelctronics and advanced materials. 5(2003)569-573.

Figure Captions:

- ✓ Fig. 1a. XRD pattern of undoped ZnO powder
- ✓ Fig. 1b. XRD pattern of 5 at % Co doped ZnO powder
- ✓ Fig. 1c. XRD pattern of 10 at % Co doped ZnO powder
- ✓ Fig. 2a. XRD pattern of 5 at % Co doped ZnO pellet annealed at 450°C
- ✓ Fig. 2b. XRD pattern of 5 at % Co doped ZnO pellet annealed at 550°C
- Fig. 2c. XRD pattern of 5 at % Co doped ZnO pellet annealed at 650°C
- Fig. 3a. XRD pattern of 10 at % Co doped ZnO pellet annealed at 450°C
- Fig. 3b. XRD pattern of 10 at % Co doped ZnO pellet annealed at 550°C
- ✓ Fig. 3c. XRD pattern of 10 at % Co doped ZnO pellet annealed at 650°C
- ✓ Fig. 4a. EDX spectrum of undoped ZnO powder
- ✓ Fig. 4b. EDX spectrum of 5 at % Co doped ZnO powder
- Fig. 4c. EDX spectrum of 10 at % Co doped ZnO powder
- ✓ Fig. 5a. SEM image of undoped ZnO powder
- ✓ Fig. 5b. SEM image of 5 at % Co doped ZnO powder
- ✓ Fig. 5c. SEM image of 10 at % Co doped ZnO powder
- ✓ Fig. 6a. SEM image of 5 at % Co doped ZnO pellet annealed at 450°C
- Fig. 6b. SEM image of 5 at % Co doped ZnO pellet annealed at 550°C
- ✓ Fig. 6c. SEM image of 5 at % Co doped ZnO pellet annealed at 650°C
- ✓ Fig. 7. Absorption spectrum of undoped and 5, 10 at.wt % Co doped ZnO powder
- ✓ Fig. 8a. TEM image of Co doped ZnO powder
- ✓ Fig. 8b. HR-TEM image of Co doped ZnO powder
- ✓ Fig. 9a. Activation energy of undoped ZnO annealed at 450°, 550° &650°C
- ✓ Fig. 9b. Activation energy of 5 at % Co doped ZnO pellet annealed at 450°, 550° & 650°C
- ✓ Fig. 9c. Activation energy of 10 at % Co doped ZnO pellet annealed at 450°, 550° & 650°C